

# 1     **Deep Dive into Hydrologic Simulations at Global Scale: Harnessing the Power of Deep** 2     **Learning and Physics-informed Differentiable Models ( $\delta$ HBV-globe1.0-hydroDL)**

3     Dapeng Feng<sup>1,2,3</sup>, Hylke Beck<sup>4</sup>, Jens de Bruijn<sup>3,5</sup>, Reetik Kumar Sahu<sup>3</sup>, Yusuke Satoh<sup>6</sup>, Yoshihide Wada<sup>7</sup>,  
4     Jiangtao Liu<sup>1</sup>, Ming Pan<sup>8</sup>, Kathryn Lawson<sup>1</sup>, Chaopeng Shen<sup>1\*</sup>

5  
6     <sup>1</sup> Civil and Environmental Engineering, Pennsylvania State University, University Park, PA, USA

7     <sup>2</sup> Earth System Science, Stanford University, Stanford, CA, USA

8     <sup>3</sup> Water Security Research Group, International Institute for Applied Systems Analysis (IIASA), Laxenburg, Austria

9     <sup>4</sup> Climate and Livability Initiative, Physical Science and Engineering Division, King Abdullah University of Science and  
10    Technology, Thuwal, Saudi Arabia

11    <sup>5</sup> Institute for Environmental Studies (IVM), Vrije Universiteit Amsterdam, Amsterdam, Netherlands

12    <sup>6</sup> Moon Soul Graduate School of Future Strategy, Korea Advanced Institute of Science and Technology, Daejeon, Republic of  
13    Korea

14    <sup>7</sup> Climate and Livability Initiative, Center for Desert Agriculture, Biological and Environmental Science and Engineering  
15    Division, King Abdullah University of Science and Technology, Thuwal, Saudi Arabia

16    <sup>8</sup> Center for Western Weather and Water Extremes, Scripps Institution of Oceanography, University of California San Diego,  
17    La Jolla, CA, USA

18    \*Correspondence to: Chaopeng Shen (cshen@enr.psu.edu)

19    **Abstract.** Accurate hydrological modeling is vital to characterizing how the terrestrial water cycle responds to climate change.  
20    Pure deep learning (DL) models have shown to outperform process-based ones while remaining difficult to interpret. More  
21    recently, differentiable, physics-informed machine learning models with a physical backbone can systematically integrate  
22    physical equations and DL, predicting untrained variables and processes with high performance. However, it was unclear if  
23    such models are competitive for global-scale applications with a simple backbone. Therefore, we use - for the first time at this  
24    scale - differentiable hydrologic models (fullname  $\delta$ HBV-globe1.0-hydroDL and shorthand  $\delta$ HBV) to simulate the rainfall-  
25    runoff processes for 3753 basins around the world. Moreover, we compare the  $\delta$ HBV models to a purely data-driven long  
26    short-term memory (LSTM) model to examine their strengths and limitations. Both LSTM and the  $\delta$ HBV models provide  
27    competent daily hydrologic simulation capabilities in global basins, with median Kling-Gupta efficiency values close to or  
28    higher than 0.7 (and 0.78 with LSTM for a subset of 1675 basins with long-term records), significantly outperforming  
29    traditional models. Moreover, regionalized differentiable models demonstrated stronger spatial generalization ability (median  
30    KGE 0.64) than a traditional parameter regionalization approach (median KGE 0.46) and even LSTM for ungauged region  
31    tests in Europe and South America. Nevertheless, relative to LSTM, the differentiable model was hampered by structural

32 deficiencies for cold or polar regions, and highly arid regions, and basins with significant human impacts. This study also sets  
33 the benchmark for hydrologic estimates around the world and builds foundations for improving global hydrologic simulations.

34

35 **Short Summary.** Accurate hydrological modeling is vital to characterizing water cycle responses to climate change. For the  
36 first time at this scale, we use differentiable physics-informed machine learning hydrologic models to simulate rainfall-runoff  
37 processes for 3753 basins around the world and compare them with purely data-driven and traditional approaches. This sets a  
38 benchmark for hydrologic estimates around the world and builds foundations for improving global hydrologic simulations.

39

40 **Key Words.** Physics-informed machine learning; Differentiable hydrologic models; Global hydrologic modeling; high  
41 resolution evaluation; Parameter regionalization; Prediction in ungauged regions

## 42 1. Introduction

43 Hydrological models are vital tools to model and elucidate the terrestrial water cycle, and have been widely used in flood  
44 forecasting (Maidment, 2017), water resources management (Jayakrishnan et al., 2005), and assessing climate change impacts  
45 (Hagemann et al., 2013). Recently, deep learning (DL) models have demonstrated superior performance compared to  
46 traditional process-based hydrological models in accurately predicting different components of the hydrologic cycle (Shen,  
47 2018), such as soil moisture (Fang et al., 2017, 2019; Fang and Shen, 2020), streamflow (Feng et al., 2020; Kratzert et al.,  
48 2019b; Konapala et al., 2020), groundwater (Wunsch et al., 2021) and water quality (Hansen et al., 2022; Rahmani et al., 2021;  
49 Saha et al., 2023; Zhi et al., 2021). Long short-term memory (LSTM) networks, which are a type of recurrent neural network  
50 (Hochreiter and Schmidhuber, 1997), are currently popular DL algorithms for handling time series dynamics in hydrology,  
51 while other architectures like transformers can also be employed. LSTM models have established state-of-the-art accuracy for  
52 streamflow prediction at continental and smaller scales (Feng et al., 2020, 2021; Kratzert et al., 2019a, b; Lees et al., 2021;  
53 Mai et al., 2022).

54

55 Although DL models have shown great prediction accuracy compared to traditional models, they usually do not possess clear  
56 physical constraints inside the model and are often considered to be “black boxes”, despite recent efforts shed by some  
57 interpretive efforts (Lees et al., 2022). Thus, purely data-driven models are limited in that they cannot predict unobservable or  
58 untrained physical variables. Therefore, a data-driven DL model impedes the investigation of the physical relations of different  
59 hydrologic variables behind the change in the target variable. In contrast, traditional process-based hydrologic models  
60 following physical laws like mass balances can provide a full set of diagnostic outputs for hydrologic variables like soil water  
61 storage, groundwater recharge, evapotranspiration and snow water equivalent, even though they are usually only calibrated on  
62 discharge observations (Burek et al., 2020; Müller Schmied et al., 2014). The multivariate output nature of these models  
63 provides an opportunity for calibration on one or more observable variables to better predict other, perhaps unobservable,

64 variables (in reality, whether this is the case or not depends on if the issue of parameter non-uniqueness is addressed). However,  
65 it seems quite difficult for the traditional physical model to approach the performance level of the DL models in daily  
66 hydrograph metrics (Feng et al., 2020; Kratzert et al., 2019b) or to improve in generalization with increasing training data  
67 (Tsai et al., 2021). In addition, traditional calibration is typically done site-by-site and can be time- and labor-intensive.  
68 Therefore, it logically follows that integrating DL and process-based models might enable harnessing their respective strengths  
69 while circumventing their weaknesses (Shen et al., 2023).

70

71 By combining a physical model with a DL model, differentiable modeling (Shen et al., 2023) provides a systematic solution  
72 to leveraging the strengths of both model types while circumventing their limitations. In differentiable models, we use process-  
73 based models as a backbone and insert neural networks to either provide parameters (Tsai et al., 2021) or process substitutes  
74 for physical models (Feng et al., 2022, 2023; Höge et al., 2022; Jiang et al., 2020; Aboelyazeed et al., 2023), or they could use  
75 limited physical constraints (Kraft et al., 2022). They are collectively called “differentiable models” in the sense that they can  
76 rapidly compute gradients of outputs with respect to inputs or parameters using automatic differentiation (or any other means).  
77 The differentiability enables the training of neural network components placed anywhere in the model via backpropagation.  
78 Inserting neural networks into process-based models can be perceived as posing questions regarding some uncertain  
79 relationships given some known ones (priors) and we want to get answers for these questions by automatically learning from  
80 big data.

81

82 Some of our recent work has applied differentiable modeling to the conceptual hydrologic model named Hydrologiska Byråns  
83 Vattenbalansavdelning (HBV) (Bergström, 1976, 1992; Seibert and Vis, 2012), and built a physics-informed hybrid model for  
84 basins in the contiguous United States (CONUS) (Feng et al., 2022, 2023). The model is “regionalized” in the sense that the  
85 embedded neural network components are trained simultaneously on all basins in the study region in order to provide physical  
86 HBV parameters which are learned from raw information of basin attributes, resulting in improved generalizability and reduced  
87 overfitting to local noise. With the help of differentiable modeling to flexibly evolve the original structure of HBV, the  
88 differentiable hybrid models can approach the performance level of the LSTM model, whilst being constrained to physical  
89 laws and keeping process clarity to predict untrained diagnostic variables with decent accuracy (Feng et al., 2022). Since the  
90 framework is regionalized, this differentiable model can be used to predict in ungauged regions and even extrapolates better  
91 spatially than LSTM in data-sparse regions when tested across the CONUS (Feng et al., 2023).

92

93 Owing to the complexity of calibration, current global hydrologic models are largely either uncalibrated (Hattermann et al.,  
94 2017; Zaherpour et al., 2018) or only calibrated on mean annual water budgets in limited regions (Burek et al., 2020; Müller  
95 Schmied et al., 2014). We desire efficient regionalized models that maximally leverage available information and provide  
96 accurate predictions to diverse basins across different climate groups and geographic characteristics in the world. We also want  
97 the models to perform decently even in data-sparse regions, showing competitive extrapolation ability, given that many large

98 regions such as in Africa and Asia lack publicly available streamflow data. DL and differentiable models seem plausible  
99 candidates for such simulations. Nevertheless, previous studies on DL and physics-informed differentiable models mainly  
100 focus on continental or smaller scales, with a relatively homogeneous forcing dataset --- it is unclear if their observed strengths,  
101 e.g., high performance and strong generalization ability, can carry over to global scales, where the climate is much more diverse  
102 and datasets differ widely in their biases and uncertainty characteristics. In particular, we want to thoroughly examine how  
103 well these models can leverage information learned in data-rich continents to characterize the hydrologic processes in  
104 ungauged regions across the world. Meanwhile, DL models also show favorable scaling relationships (or data synergy) where  
105 more data leads to more robust models (Fang et al., 2022). Thus, training on a larger dataset may provide additional benefits.

106

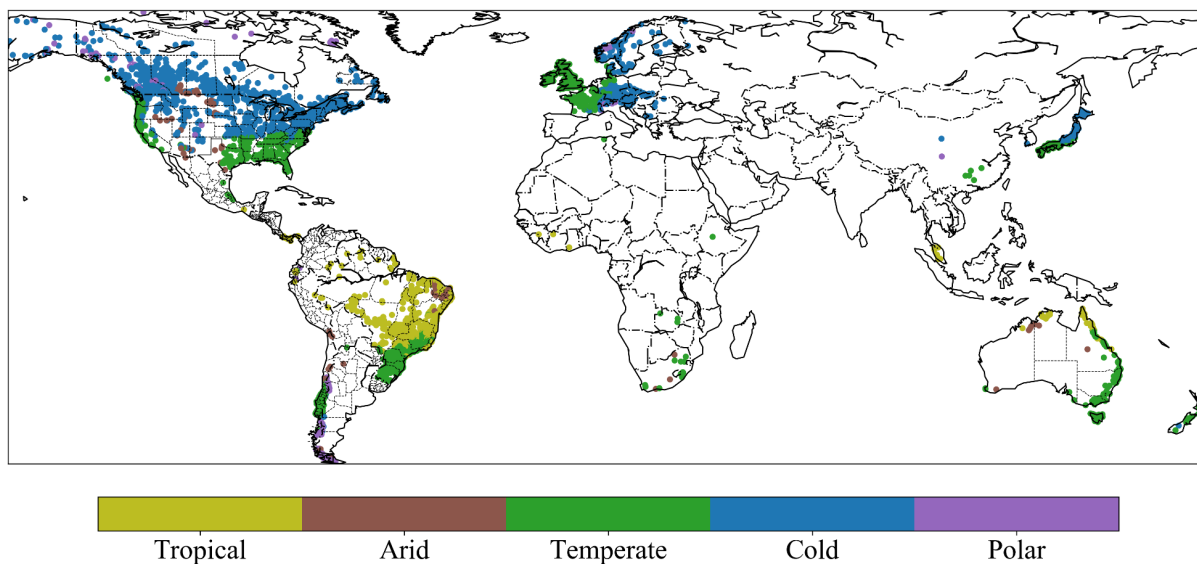
107 In this study, we test physics-informed differentiable models (with the full version name  $\delta$ HBV-globe1.0-hydroDL, where “ $\delta$ ”  
108 represents “differentiable”, globe1.0 is the version, and “hydroDL” refers to our particular code implementation.  $\delta$ HBV is  
109 used as the abbreviation in this paper) to simulate hydrologic processes for global basins and compare results to purely data  
110 driven methods and traditional modeling approach. We focus on regionalized modeling and emphasize the importance of  
111 spatial generalization in data-sparse scenarios, since observed streamflow data in many parts of the world are scarce. This  
112 means one framework with parameter regionalization from geographic attributes will be used to model all the global basins  
113 rather than calibrating a separate model in each individual basin (Beck et al., 2020b; Feng et al., 2022; Mizukami et al., 2017).  
114 We first investigate what prediction accuracy can be achieved by different models at global scale by learning from a large and  
115 diverse dataset. We then relate the global spatial patterns of model performance to geographic characteristics and hydrologic  
116 processes to identify model structural deficiencies and gain hydrologic insights. Finally, we provide evidence indicating which  
117 type of model may be more appropriate for next-generation global modeling by rigorously examining their generalizability to  
118 ungauged regions across the world.

## 119 **2. Data and methods**

### 120 **2.1 Global datasets**

121 We use a global database compiled in a previous study (Beck et al., 2020b) which contains a total of 4229 headwater  
122 catchments. The dataset includes basin mean meteorological forcings, catchment characteristics such as the climate,  
123 topography, land cover, soil composition, and geology information to support parameter regionalization, along with streamflow  
124 gauge discharge observations. Meteorological forcings are the driving inputs of hydrological models. This global dataset  
125 includes daily precipitation from Multi-Source Weighted-Ensemble Precipitation (MSWEP), a product that merges gauge,  
126 satellite, and reanalysis precipitation data (Beck et al., 2017c, 2019), and maximum and minimum temperature from Multi-  
127 Source Weather (MSWX), a product that bias-corrects and harmonizes meteorological data from atmospheric reanalyses and  
128 weather forecast models (Beck et al., 2022). Potential evapotranspiration was estimated using the method from Hargreaves  
129 (1994). The discharge observations at the outlet gauges were used as prediction targets to train the hydrologic models. We

130 excluded some basins with potential erroneous discharge records such as showing unreasonable magnitude way larger than  
131 precipitation or dramatic differences between two time intervals, by manually performing visual screening, and also excluded  
132 those with severe amounts of missing data (less than 5 years' worth of data points in the study period from 2000 to 2016).  
133 Thus, 3753 basins were finally used to evaluate different models. These basins had been classified into five Köppen-Geiger  
134 climate classes in Beck et al., (2020b), including tropical (489 basins), arid (109 basins), temperate (1423 basins), cold (1593  
135 basins), and polar (139 basins), as shown in Figure 1. To evaluate the simulations of untrained variables like evapotranspiration  
136 (ET), the MOD16A2GF (Running et al., 2021), a gap-filled 8-day composite ET product estimated from the Moderate  
137 Resolution Imaging Spectroradiometer (MODIS) satellite data and meteorological reanalysis data, were used as independent  
138 observations to compare against the simulated ET from differentiable hydrologic models.



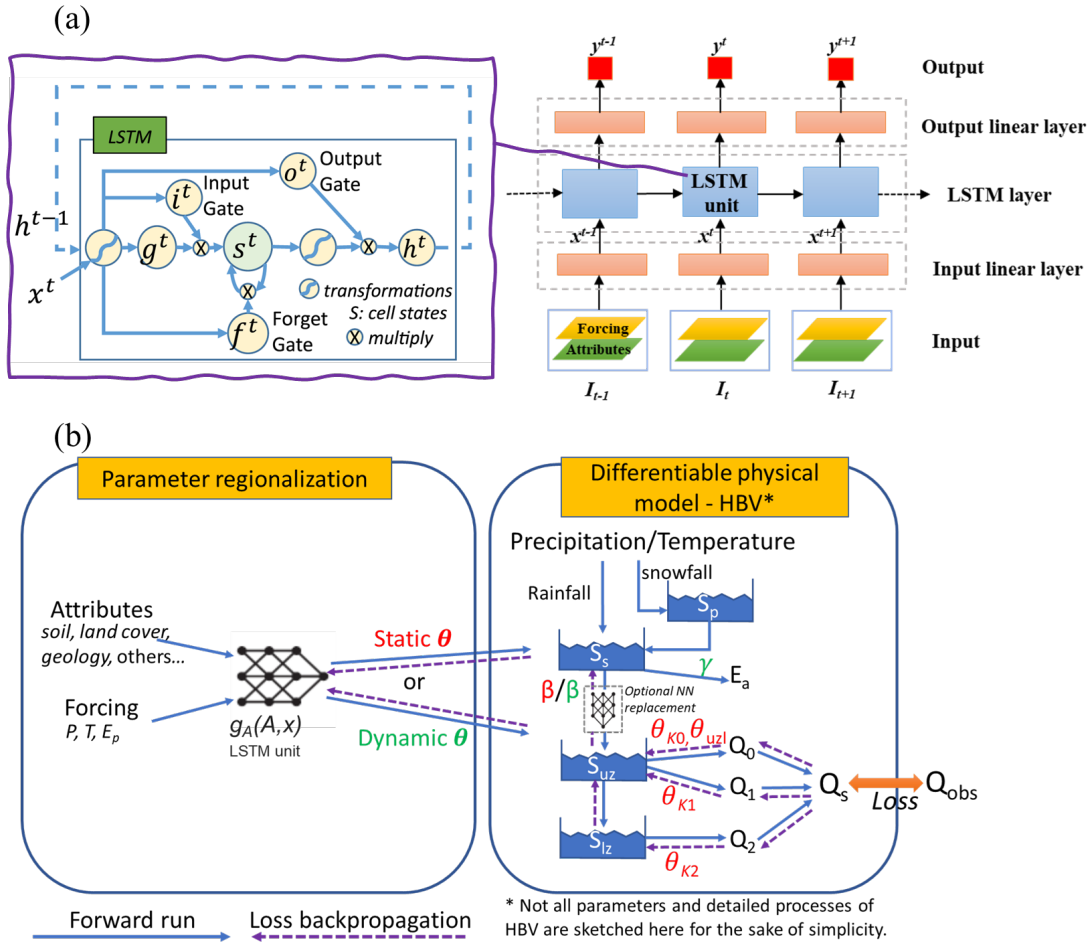
139

140 *Figure 1. Locations and climate groups of the 3753 global basins used in this study, which were originally compiled by Beck et al., 2020.*  
141 *Plotted in Python using Matplotlib Basemap Toolkit.*

## 142 2.2 The long short-term memory (LSTM) streamflow model for comparison

143 Here the LSTM model is used as a benchmark for purely data-driven DL. The LSTM has “cell states” and “gates” to maintain  
144 and filter information, as shown in Figure 2a. The input, forget, and output gates control the flow of information, respectively  
145 controlling what to let in, what to forget, and what to output from the system. In this study we use the LSTM streamflow model  
146 demonstrated in Feng et al. (2020) which has been successfully applied to simulate streamflow in hundreds of basins across  
147 the CONUS. The framework takes meteorological forcings and basin attributes as inputs and generates daily streamflow  
148 predictions for each basin at each time step (Figure 2a). We used mini-batches to train the LSTM model, where each minibatch  
149 was composed of two-year sequences from 256 randomly-selected basins. The first-year sequences are only used for  
150 initializing the cell states, so we calculate the batch loss function only on the second-year sequences. The training sequences  
151 were also randomly selected from the whole training period, and one epoch was finished when the model had seen all the

152 training data. Note that this sequence length is a subset of, and different concept from, the length of training period. Sequence  
 153 length specifically refers to the length of the training instance that comprises a minibatch, whereas training period refers to the  
 154 whole period when observations are available for training, from which the minibatch sequence length is randomly selected.  
 155 The model was forwarded on each minibatch iteratively and its weights were updated using gradient descent after each  
 156 forwarding. One epoch was considered to have occurred when the model is iterated over all the training data. We trained the  
 157 LSTM model for 300 epochs to achieve convergence.



158

159 **Figure 2. Illustrations of two different types of regionalized hydrologic models. (a) Framework of the purely data-driven LSTM**  
 160 **streamflow model (adapted from Figure 2 in Feng et al., 2020), and (b) framework of the differentiable HBV model ( $\delta$ HBV-globe1.0-**  
 161 **hydroDL) with parameter regionalization developed in Feng et al. (2022) (adapted from Figure 1 in Feng et al. (2022)). The neural**  
 162 **network  $g_A$  here is a LSTM unit which is trained by the observed streamflow to produce the static or dynamic physical HBV parameters**  
 163 **( $\theta, \beta, \gamma$ ) from basin characteristics.**

### 164 2.3 The hybrid differentiable hydrologic models

165 We used the hybrid differentiable models ( $\delta$ HBV-globe1.0-hydroDL) developed in Feng et al., (2022) for regionalized  
166 modeling in global basins. The HBV model used here as the physical backbone is a conceptual hydrologic model with  
167 representations of snowpack, soil, and groundwater storages, and can simulate flux variables such as snow melting,  
168 evapotranspiration, and quick and slow outflows (Beck et al., 2020b; Bergström, 1976, 1992; Seibert and Vis, 2012). The  
169 differentiable parameter learning (dPL) framework (Tsai et al., 2021) is used to provide parameter regionalization for HBV,  
170 as shown by the  $g_A$  neural network in Figure 2b. The  $g_A$  network, which is a LSTM unit here, takes basin attributes and  
171 meteorological forcings as inputs, and outputs static or dynamic physical HBV parameters. The differentiable HBV model  
172 then takes these parameters as well as the meteorological forcings to simulate the hydrological process and predict daily  
173 streamflow discharge along with other key flux variables. The whole framework including HBV itself was implemented in a  
174 DL platform (PyTorch 1.0.1 was used for the original development and the model has also shown good compatibility with  
175 more recent PyTorch versions, (Paszke et al., 2017)) supporting automatic differentiation and trained with gradient descent to  
176 minimize the difference between the simulated and observed streamflow (the loss function). As in Feng et al., (2022), we  
177 employed the loss function based on root-mean-square error (RMSE) with two weighted parts. The first part calculates RMSE  
178 directly on the simulated and observed discharge, while the second part calculates RMSE on the transformed discharge records  
179 to improve low flow representations. Note that we do not directly train the HBV parameters; rather, we focus on training the  
180 weights of the  $g_A$  neural network to map the relationship between basin-averaged characteristics and HBV parameters.

181

182 As described in Feng et al. (2022), the differentiable modeling framework enables optional modification of the structures of  
183 the original HBV model to enable better performance and we use two versions of evolved HBV models in this study. We used  
184 16 parallel subbasin-scale response units, each with a separate set of parameters to describe a fraction of the basin with different  
185 hydrologic responses. These components implicitly represent subbasin-scale spatial heterogeneity. The simulated fluxes (e.g.,  
186 streamflow) are the average of all the response units. The parameters of the multiple components are different and all are  
187 produced simultaneously by the same  $g_A$  network. The first version of our model (referred to as “dPL + evolved HBV”) only  
188 has static parameters which are kept constant during the hydrologic simulation. The second version (referred to as “dPL +  
189 evolved HBV with DP) further allows some formerly static parameters of the multi-component model to vary daily with the  
190 meteorological forcings. These dynamic parameters (DP) were also produced by the  $g_A$  LSTM unit. If we were to apply the  
191 dynamic parameterization to all parameters, the model could become overly flexible, potentially leading to overfitting to the  
192 training data (which would lead to issues with extrapolation beyond the training data). To reduce the risk of overfitting, we  
193 restricted the dynamism to only two empirical parameters: the shape coefficient  $\beta$  in the equation that describes the  
194 relationships between soil storage and potential runoff, and a newly added shape parameter ( $\gamma$ ) which is involved in the  
195 calculation of evapotranspiration. For more details regarding these differentiable HBV models, please refer to our previous  
196 studies (Feng et al., 2023, 2022).

## 197 **2.4 Experiments and evaluation metrics**

198 We ran one temporal and two spatial generalization experiments to evaluate the performance of different regionalized models.  
199 For the temporal generalization experiment, the models were trained for the period of 2000 to 2016 on all global basins, and  
200 tested for the period of 1980 to 1997. Without spatially holding out any basin during training, this experiment aimed at  
201 evaluating the model’s generalizability in the time dimension by testing prediction ability on the same basins but in a different  
202 time period from the training data. The other two spatial generalization experiments served as the true litmus tests for  
203 evaluating the effectiveness of regionalization schemes, i.e., how well the model can be applied to basins that have never been  
204 seen during training. The first spatial generalization experiment was a traditional “prediction in ungauged basins” (PUB)  
205 problem, where we randomly divided the whole global basin set into 10 folds (groups) and performed cross-validation across  
206 these folds to obtain spatial out-of-sample predictions for all basins (training on 9 of the folds with the 10th fold held out and  
207 testing on the 10th, then rotating such that each fold is used for testing once). The second spatial generalization experiment,  
208 which we refer to as cross-continent “prediction in ungauged regions” (PUR), was more challenging. In this experiment, we  
209 assumed that all the basins in certain continents are ungauged and excluded from the training dataset, trained a regionalized  
210 model in other data-rich continents, and then tested the trained model to make predictions in the ungauged continents. With  
211 random hold-out, an ungauged test basin in the first spatial generalization experiment always has training gauges surrounding  
212 it. Therefore, the first PUB experiment can be interpreted as spatial interpolation. The second spatial experiment (cross-  
213 continent PUR) holds out all the basins in one continent as testing targets, and thus is the much harder test of spatial  
214 extrapolation.

215

216 To evaluate the overall performance of the hydrologic models, we used the Kling-Gupta Efficiency (KGE; (Gupta et al., 2009;  
217 Kling et al., 2012) as compared in Beck et al., (2020b) and Nash-Sutcliffe Efficiency (NSE; (Nash and Sutcliffe, 1970). KGE  
218 has three components that account for correlation, mean bias, and variability bias, while NSE mainly represents the variance  
219 explained by the simulations. Both metrics indicate better performance when their values are closer to the maximum value of  
220 1. We also examined the percent bias of the top 2% peak flow range (FHV) and bottom 30% low flow range (FLV) of  
221 streamflow predictions to evaluate the model’s ability to simulate extreme events (Yilmaz et al., 2008). All the reported  
222 performance metrics in this study are from model evaluation on the testing dataset, which is not seen by the model during the  
223 training process.

## 224 **3. Results and discussions**

### 225 **3.1 General patterns over global basins**

226 From the standpoint of daily hydrograph metrics (KGE and NSE), LSTM and the two differentiable models all achieved highly  
227 competitive performance for the global basins in the temporal test (trained and tested on the same basins, but in different time



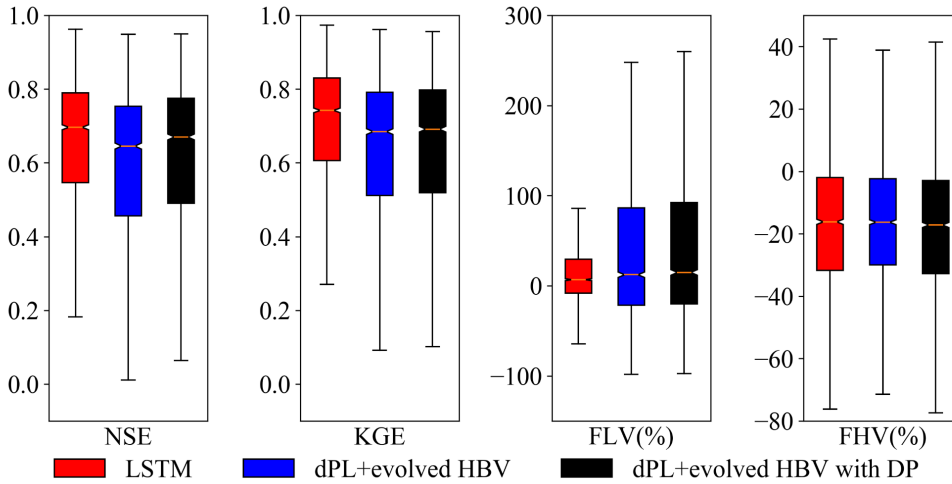
228 periods) (Figure 3). For the global dataset, all three models obtained median KGE values close to or higher than 0.7, but the  
229 LSTM model performed the best of the three models here, achieving a median NSE (KGE) value of 0.70 (0.74) for all the  
230 evaluated basins. For a subset of 1675 basins with long-term records (at least 15 years' worth of streamflow data available in  
231 the training period and 5 years' worth of data available in the testing period, though not necessarily continuous), LSTM even  
232 reached a KGE of 0.78. Both versions of the differentiable models approached the performance level of the LSTM, in  
233 agreement with our previous assessment for the CONUS (Feng et al., 2022). The model with dynamic parameters achieved a  
234 median NSE (KGE) of 0.67 (0.69), followed by the model with static parameters, which obtained a median NSE (KGE) of  
235 0.65 (0.68).

236

237 The LSTM exhibited advantages for the low flow predictions compared with the differentiable models, as shown by the FLV  
238 metric (Figure 3). However, for the peak flow predictions, the LSTM and differentiable models were quite similar, and they  
239 all underestimated the observed peaks (FHV in Figure 3). The underestimation for peak flows is consistent with what was  
240 found in previous studies. For example, all the physical and deep learning models have significant negative peak flow bias  
241 when benchmarked in the CONUS dataset (Feng et al., 2020; Kratzert et al., 2019b). We hypothesize that the systematic  
242 underestimation of peaks may be partially related to bias in precipitation forcings. MSWEP is based on the ERA5 reanalysis,  
243 which is known to underestimate precipitation peaks (Beck et al., 2019). Furthermore, the use of basin-averaged, daily-  
244 averaged precipitation may further suppress the peaks (Chen et al., 2017). In addition, the errors with peak flow could also be  
245 partly due to some numerical and structural issues with the differentiable models, e.g., numerical errors introduced by the  
246 explicit and sequential solution scheme of HBV with excessive use of threshold functions that lead to different results when  
247 the sequence changes, and structure limitations, e.g., deeper groundwater storage cannot feed back to the upper layers. Given  
248 the commonality of this issue, we call for community efforts and collaboration to address this issue.

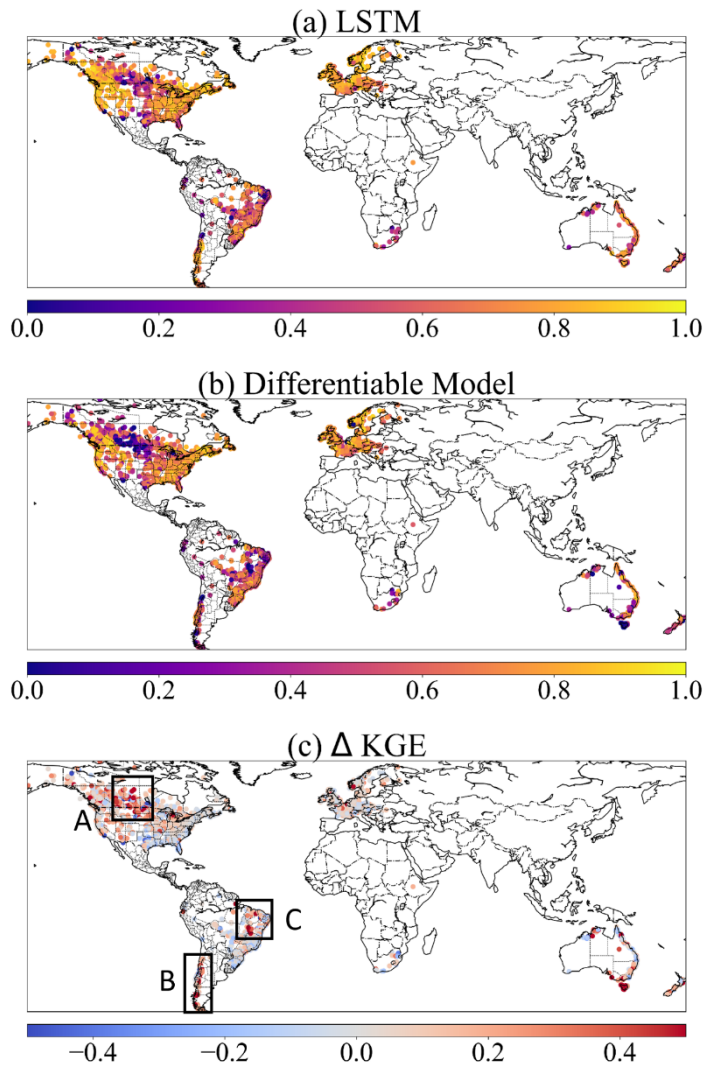
249

250 Both the LSTM model and the differentiable models performed well over diverse landscapes, including North America  
251 (especially along the Rocky and Appalachian mountain ranges and the Southeastern Coastal Plains), Western Europe, Asia  
252 (mostly Japan), the southern part of Brazil, and the northeast coast of Australia (Figure 4a and b). There are other regions  
253 where none of the three models performed well, such as the longitudinally-central part of North America (Great Plains and  
254 Interior Lowlands), the southern edge of Chile (with many glaciers), the Tasmania state of Australia, and the few basins in  
255 Africa. These regions, for example, the Northern Great Plains and the state of Texas in the CONUS, have always been difficult  
256 for all kinds of models, likely due to incorrect basin boundary, highly localized precipitation, the dry conditions with small  
257 runoff amounts and flash flooding mechanisms (Berghuijs et al., 2014; Driscoll et al., 2002; Feng et al., 2020; Martinez and  
258 Gupta, 2010; Newman et al., 2017), to be explored below. Despite some challenges, however, these values represent currently  
259 the best metrics reported at the global scale compared to earlier studies, e.g., (Alfieri et al., 2020; Beck et al., 2020b, 2017a;  
260 Hou et al., 2023), attesting to these models' great potential as global modeling tools.



262

263 *Figure 3. Performance comparison between the LSTM and differentiable models on global basins. dPL refers to the differentiable*  
 264 *parameter learning framework, while “evolved HBV” refers to some modifications to improve the standard HBV model, and “with DP”*  
 265 *indicates that some parameters were allowed to be dynamic rather than static. Here, the horizontal line inside the colored box represents*  
 266 *the median, while the top and bottom of the colored box indicate the first and third quartiles. The bars extending from the colored boxes*  
 267 *indicate 1.5 times the interquartile range from the first and third quartiles. NSE is Nash-Sutcliffe Efficiency, KGE is Kling-Gupta*  
 268 *Efficiency, FLV indicates the model’s percent bias on the bottom 30% low flow range of streamflow, and FHV indicates percent bias on*  
 269 *the top 2% peak flow range of streamflow.*



270

271 *Figure 4. The spatial patterns of different model performance and their differences shown by KGE metric. (a) the LSTM model; (b) the*  
 272 *differentiable model with dynamic parameters (dPL + evolved HBV with DP); and (c) the KGE difference between two models (KGE of*  
 273 *LSTM – KGE of dPL + evolved HBV with DP). Plotted in Python using Matplotlib Basemap Toolkit.*

### 274 3.2 Model behaviors and limitations across climate groups and regions

275 All three models' performances vary significantly across different climate groups of the global basins (Figure 5), revealing  
 276 their strengths and limitations. The LSTM model behaved the best in the polar, cold, and temperate groups, while the  
 277 performance deteriorated in the tropical and arid basins. Similar to LSTM, differentiable models showed strong performance  
 278 in temperate and cold groups and worse performance in tropical ones, with the worst performance in arid basins. These clusters  
 279 of challenging basins can also be identified on the map (Figure 4a and b). As we examine how LSTM and differentiable models

280 behave differently, we find that such differences can be attributed to processes missing from the simple backbone process-  
281 based model (HBV here) as explained below. Here we use LSTM as an indicator of upper bound, that is, it shows the ideal  
282 performance of a model, given the available information from forcing and input data. Thus the distance from LSTM indicates  
283 either systematic and predictable forcing errors (which can be remediated by LSTM) or structural issues with the differentiable  
284 model.

285

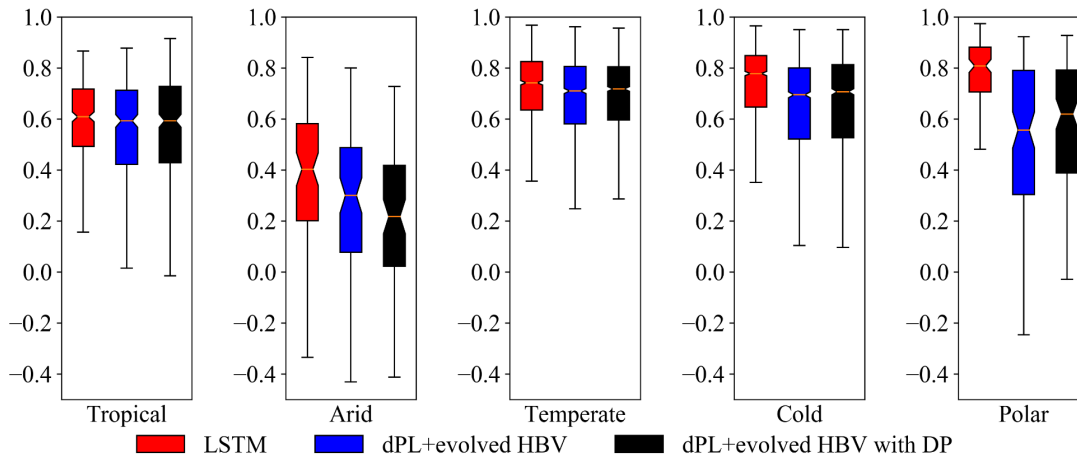
286 For example, the polar group stands out as a climate type favoring LSTM, while the cold group shows a similar but less  
287 pronounced contrast, both of which may be related to HBV's physical deficiencies and forcing issues with snow undercatch.  
288 For the polar (cold) groups, LSTM surprisingly had a median KGE of 0.81 (0.78) while the differentiable model only reached  
289 0.62 (0.71). The polar regions include, for example, Southern Chile (in region B in Figure 4c). As glaciers can store water for  
290 extended periods of time and are driven mostly by temperature rather than rainfall, it is possible for LSTM to capture the  
291 temperature-driven dynamics (Lees et al., 2022) while the original HBV itself does not have a glacial module. HBV does not  
292 have the ability to simulate frozen soil, sublimation or snow cover fractions. Furthermore, as snow gauges in high altitude are  
293 known to suffer systematic bias due to undercatch problems (Beck et al., 2020a), LSTM can learn to address such systematic  
294 bias while physical differentiable models cannot due to mass balance. For the cold regions, e.g., high-latitude regions of the  
295 North American Great Plains (Region A in Figure 4c --- this also includes the Prairie Pothole Region, or PPR), HBV may  
296 suffer from not having descriptions for frozen ground conditions (soil ice) which can influence infiltration, and rainfall  
297 underestimation due to undercatch, ice blockage, and other potential reasons (Beck et al., 2020a). In addition, another reason  
298 why LSTM and differentiable HBV may have trouble with PPR (but HBV performed especially poorly) is the countless  
299 wetlands that store water until full and become connected after snowmelt and large rainfall. HBV does not have modules that  
300 can describe such large-scale fill-connect-spill processes (Shaw et al., 2013; Vanderhoof et al., 2017).

301

302 A more prominent challenge is the arid regions (middle CONUS, north Chile and east Brazil in Figure 1 and Figure 4). This  
303 challenge can be attributed to the long duration of low flows which requires long-term memory, and flash floods which result  
304 from intense short-duration storms not well represented at the daily scale. Even the LSTM model cannot retain year-long  
305 memory and cannot perform well for the baseflow (Feng et al., 2020). Because HBV has a linear reservoir for its slow-flow  
306 (lowest) bucket, it cannot generate zero base flows. Neither can it well simulate the impact of intense hourly-scale rainfall.  
307 These process improvements need to be considered in the future. Another reason for the challenge in arid regions is the lack  
308 of reservoir management modules. Arid regions tend to have water management infrastructure that significantly influences  
309 streamflow (Veldkamp et al., 2018). Since the HBV model doesn't have any module representing human impacts on the natural  
310 water cycle, the poor performance in middle Brazil in region C may have come from the missing representation of human  
311 interferences. There are large population and intensive agricultural activities in this region which could induce significant  
312 impacts on the hydrologic process. Parameter compensations apparently cannot make up for all the missing mechanisms.

313

314 The sensitivity of model performance to missing processes in the differentiable models is both good and bad news. It’s good  
 315 news because this means we can identify suitable or insufficient process representations by learning from data. On the other  
 316 hand, this means more challenges as we need to increase the process complexity of this model before it can perform well for  
 317 these basins, unlike the purely data-driven LSTM which is not explicitly concerned with physical processes.



318

319 *Figure 5. The performance comparison (KGE, Kling-Gupta Efficiency) of different models for five climate groups. dPL refers to the*  
 320 *overall differentiable parameter learning framework, while “evolved HBV” refers to some modifications to improve the standard HBV*  
 321 *model, and “with DP” indicates that some parameters were allowed to be dynamic rather than static. Here, the horizontal line inside the*  
 322 *colored box represents the median, while the top and bottom of the colored box indicate the first and third quartiles. The bars extending*  
 323 *from the colored boxes indicate 1.5 times the interquartile range from the first and third quartiles.*

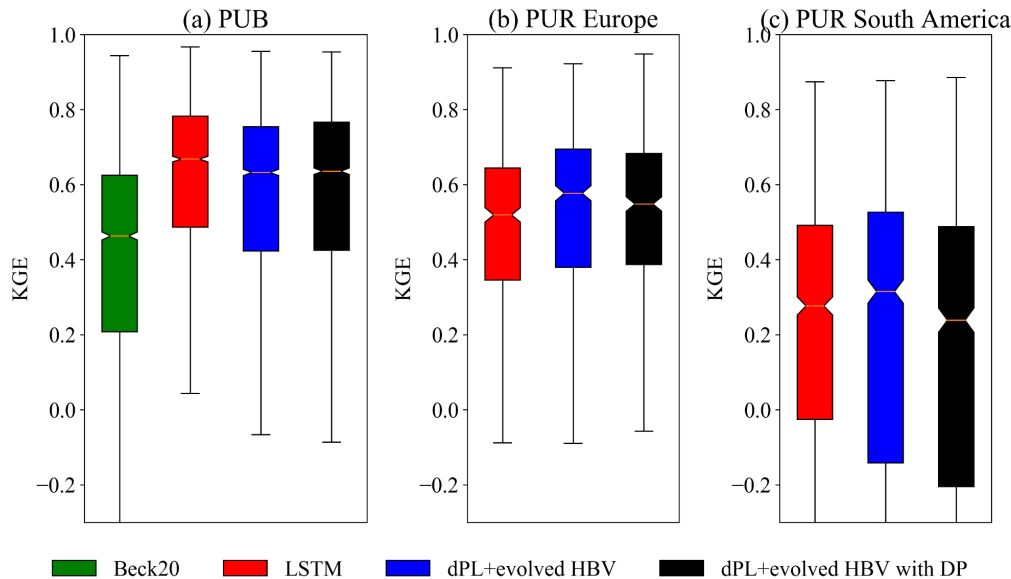
### 324 3.3 Spatial generalization for prediction in ungauged regions

325 While LSTM maintains mild advantages over differentiable models in data-dense settings, it was outperformed by  
 326 differentiable models in a highly data-scarce scenario. As mentioned above, the data-dense setting was tested in the randomized  
 327 holdout test called prediction in ungauged basins (PUB), while the data-scarce scenario was tested in the regional holdout test,  
 328 or prediction in ungauged regions (PUR). In the global PUB test, LSTM has a small edge (median KGE=0.67) over  
 329 differentiable models (median KGE=0.64). Both were noticeably higher than the traditional regionalization method using  
 330 linear transfer functions reported by Beck et al. (2020b) (Beck20, median KGE=0.46), which already represents the previous  
 331 state-of-the-art performance of global parameter regionalization. Differentiable modeling does not rely on strong assumptions  
 332 of the functional form for the parameter transfer function. It leverages the powerful ability of neural networks to represent  
 333 complicated functions, and automatically learns robust and generalizable relationships between geographic attributes and  
 334 physical model parameters from large data. Therefore, we can expect significant performance advantages from differentiable  
 335 modeling compared to traditional methods relying on linear transfer functions. In the PUR scenario where European basins  
 336 were held out for testing, differentiable models (median KGE=0.58) performed significantly better than LSTM (median  
 337 KGE=0.52). In the South American PUR experiment, lower performance was seen for all models which can be expected  
 338 considering the prediction difficulties in this region even for the in-sample scenario (Region B and C in Figure 4). The median

339 KGE of LSTM is 0.28 while the differentiable model with static parameters achieves a higher median KGE of 0.31 for the  
 340 PUR scenario. It seemed that the differentiable model with dynamic parameterization was somewhat overfitted in this case,  
 341 resulting in a median KGE that was lower than the static-parameter differentiable model. We do not have PUR results from  
 342 traditional models available to compare against, since this is a very challenging issue for traditional regionalization methods  
 343 to make predictions across continents.

344

345 With these results, we show that differentiable models have demonstrated a robust capability for spatial generalization that  
 346 cannot be obtained by straightforwardly training models on data alone. This conclusion was not only verified in the USA, but  
 347 now has also been confirmed in cross-continent predictions in Europe and South America, each of which have unique  
 348 conditions with respect to data density and errors.



349

350 *Figure 6. The performance comparison (KGE, Kling-Gupta Efficiency) of different models for spatial generalization tests. (a) Random*  
 351 *hold-out test for prediction in ungauged basins (PUB), (b) and (c) holding out all the basins in Europe or South America, respectively,*  
 352 *for cross-continent predictions in ungauged regions (PUR). Beck20 refers to a traditional regionalization method using linear transfer*  
 353 *functions (Beck et al., 2020b), LSTM is the purely data-driven long short-term memory network, dPL refers to the differentiable*  
 354 *parameter learning framework, while “evolved HBV” refers to some modifications to improve the standard HBV model, and “with DP”*  
 355 *indicates that some parameters were allowed to be dynamic rather than static. Here, the horizontal line inside the colored box represents*  
 356 *the median, while the top and bottom of the colored box indicate the first and third quartiles. The bars extending from the colored boxes*  
 357 *indicate 1.5 times the interquartile range from the first and third quartiles.*

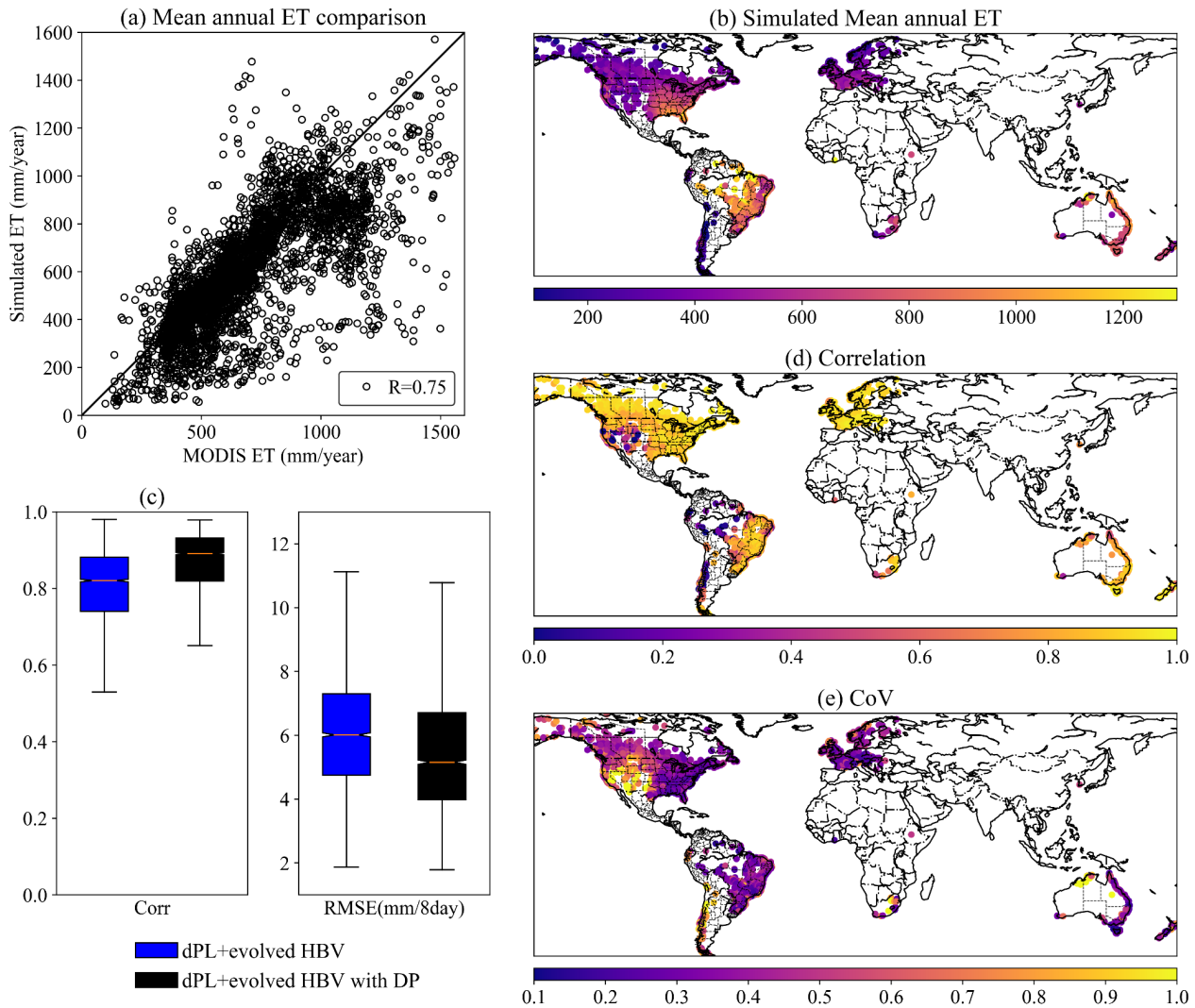
### 358 3.4 Predicting untrained variables

359 The evapotranspiration (ET) simulations from differentiable models are consistent with independent MODIS satellite estimates  
 360 of ET in both temporal dynamics and spatial patterns. We did not use any ET observations as training targets to supervise the  
 361 differentiable models. At the global scale, the mean annual ET comparison shows overall consistency with MODIS, with most

362 basins lying close to the 1:1 line and a correlation of 0.75 for all the basins (Figure 7a). Spatially, the model was able to  
363 represent energy limitations in the cold regions, e.g., high-latitude North America and Europe, and water limitations, e.g.,  
364 southwestern US and arid basins of Australia (Figure 7a and b). The model also represented high ET in basins adjacent to the  
365 Amazon forest, those along the US southeastern and Australian coast. Temporally, the median correlation of ET time series  
366 between simulations and MODIS products achieves 0.82 and 0.89 for two differentiable models in 3753 basins, respectively  
367 (Figure 7c).

368

369 The ET simulations show high correlation with MODIS in most North American and European basins (Figure 7d), in line with  
370 the good performance of streamflow modeling in these regions. However, the correlation is relatively lower in South America  
371 but the coefficient of variation of ET residuals (CoV, the ratio of standard deviation of ET residuals to the annual mean) is also  
372 small (Figure 7e), in part because the ET here is large and less driven by the seasonal energy cycle (Niu et al., 2017). MODIS  
373 ET itself is not the ground truth and always has large uncertainties in Amazonia regions due to the cloud coverage and  
374 difficulties for observation (Hilker et al., 2015; Xu et al., 2019). Furthermore, the simulations could be negatively influenced  
375 by the data quality issues with streamflow records in these regions. Upon examining the records, some stations in South  
376 America show unrealistic hydrographs that may indicate data processing errors. To address such issues in the future, more in-  
377 depth data screening and correction or constraining the model using datasets other than streamflow, e.g., eddy covariance flux  
378 data, should be considered. The CoV is less than 0.3 for most of the world, showing that ET errors are mostly small relative to  
379 its annual averages (Figure 7e). Noticeable exceptions are US southwest, where ET varies strongly from year to year and is  
380 highly dependent on the precipitation, and Chile, where glaciers and deserts are both present, posing challenges to the model.  
381 As the present study is basin-focused, we will leave the evaluation of global gridded ET to future work.



382

383 *Figure 7. The comparison between simulated ET from the differentiable hydrologic models and independent MODIS ET product. (a)*  
 384 *mean annual ET comparison, (b) simulated mean annual ET for global basins, (c) boxplots for the temporal dynamic evaluation by*  
 385 *correlation and RMSE, (d) correlation and (e) coefficient of variation for ET comparison in global basins. Maps plotted in Python using*  
 386 *Matplotlib Basemap Toolkit.*

### 387 3.5 Further discussion

388 Some central differences exist between the differentiable modeling approach and the traditional calibration approach: First,  
 389 we always attempt to train differentiable models over a large collection of sites, improving the robustness and efficiency of  
 390 learning. Second, we reimplemented the model onto PyTorch in a parallel fashion, and were thus able to leverage the high  
 391 concurrency and computing power offered by modern GPUs. Third, the commonalities between sites and the accumulation of  
 392 knowledge in the neural network further improves the efficiency of training compared to traditional training done individually



393 for each site, as the knowledge learned from one batch is inherited when the neural network is trained on the next batch. Fourth,  
394 differentiable models can flexibly evolve the structure of the physical backbone. The two types of differentiable models used  
395 in this study have used multiple parallel components per basin to represent subbasin-scale heterogeneity. For the models with  
396 dynamic parameterization, two parameter values vary at each daily time step as a function of the meteorological forcings. It  
397 seems unrealistic to use traditional parameter calibration to optimize these models with evolved structures. However,  
398 leveraging automatic differentiation and gradient descent, differentiable models can automatically learn to produce large  
399 amounts of parameters from geographic attributes through the embedded neural networks.

400

401 The challenges facing differentiable models include not only missing processes like reservoir management, ground ice, and  
402 glaciers, but also large errors in forcing and streamflow target. Substantial bias could exist in precipitation, e.g., due to snow-  
403 gauge undercatch (Hou et al., 2023), or in discharge, e.g., streamflow are measured using different approaches which exhibit  
404 large variability; for another example, gridded climate forcing data often consistently underestimate the magnitudes of heavy  
405 storms (Beck et al., 2017b). While LSTM can easily adapt to systematic bias, such forcing errors put the differentiable models  
406 under stress because they cannot reconcile streamflow observations with such forcings given the constraint of mass balances.  
407 If our objective is to learn core physics and parameterizations that are reliable despite forcing discrepancies, we can set up  
408 forcing data correction layers that can, to some extent, shield the core processes from being influenced by such errors. This  
409 will be an important aspect of future work to ensure reliable prediction of future water resources.

410

411 The backbone of a differentiable process-based model thus serves as a double-edged sword: when such backbones are  
412 essentially correct, they serve as a stabilizing element of the model that mitigates overfitting and improves generalization;  
413 when they lack critical processes or when observations have large, unexplained bias, they can drag down model performance  
414 and cause compensation between processes. However, the limitations are tractable: future work can gradually incorporate  
415 critical processes and include more observations to constrain the learning process, making sure each addition is valuable and  
416 accretive. The research community collectively has already substantial experience in evolving earth system models to include  
417 many processes. We expect some processes to be invited back in the differentiable modeling framework. Nevertheless, with  
418 differentiable modeling, we now have a new tool that was not previously available: highly flexible deep neural networks that  
419 can be placed anywhere in the model, which provide a systematic way of managing model complexity. With their help, such  
420 model evolution may take much less time than previously required.

421

422 This study builds a benchmark and a basis for model selection and diagnosis for the next-generation global hydrologic  
423 modeling, which previously did not learn from such large observations. With rigorous tests at global scale, this study proves  
424 that differentiable models are strong candidates as global water models. With powerful spatial generalization ability, they can  
425 be applied to characterizing the hydrologic processes in ungauged regions by leveraging learned information in data-rich  
426 continents. Differentiable models in this study have already learned the generalizable and robust relationships between

427 geographic attributes and physical model parameters from thousands of global catchments. Therefore, these models can be  
428 easily applied towards providing seamless global hydrologic modeling with parameters directly generated from worldwide  
429 geographic attributes. Future work can use such models to produce global hydrologic fluxes while enhancing some process  
430 representations in extremely arid, glaciated, or heavily human-influenced basins.

#### 431 **4. Conclusions**

432 In this work, we used both purely data-driven models and, for the first time, physics-informed, differentiable models to simulate  
433 rainfall-runoff processes in 3753 global basins. Both types of models achieved overall highly competitive performance for  
434 global basins with diverse climate conditions, yielding median KGE values close to or higher than 0.7 which is state-of-the-  
435 art at this large scale. The LSTM still achieved the best performance for the temporal generalization test, but the differentiable  
436 HBV models with evolved structure ( $\delta$ HBV-globe1.0-hydroDL) approach the LSTM's performance level. Furthermore, the  
437 spatial generalization experiments highlighted the stronger regionalization and extrapolation ability of differentiable models  
438 than LSTM, demonstrating its promise to be applied to data-scarce regions in the world. Routing is not included in this work  
439 and will be investigated in the future, possibly also with differentiable approaches (Bindas et al., 2022).

440

441 Different models appear to have generally consistent spatial performance patterns, though obvious distinctions stand out in  
442 several local regions. All models achieve good performance in the temperate and cold climate groups, while they all behave  
443 unsatisfactorily in the arid group. For the polar group, the differentiable model performed significantly worse than the LSTM.  
444 Without any physical constraints, LSTM shows strong power in simulating storage (snow and glacier) dominated processes,  
445 while differentiable models are limited by the structure of their physical backbone model, which in this case does not simulate  
446 multiyear ice buildup and melt. Another limitation could be soil sealing processes in extremely arid regions. These regional  
447 performance comparisons thus reveal some deficiencies of the physical backbone in  $\delta$ HBV that cannot be mitigated even by  
448 advanced neural network-based parameterization. These insights provide directions for future improvements. Different from  
449 purely data-driven models only trained by the target variable, differentiable models constrained by the physical backbone can  
450 give accurate simulations for a full set of hydrologic variables in the water cycle including evapotranspiration, snow water  
451 equivalent, water storage, infiltration and baseflow. As some process limitations are addressed in the future, we believe  
452 differentiable models will be strong candidates for the next generation global water models to characterize and predict the  
453 hydrologic processes in ungauged regions across the world.

#### 454 **Author contributions**

455 DF and CS conceived this study. DF set up the hydrologic models and ran all the experiments. DF and CS performed the major  
456 analysis, with HB, JdB, RKS, YS, YW and MP contributing substantially to the discussions on the methodology and results.

457 HB provided the global dataset and the benchmark results from a traditional regionalization scheme. JL prepared the ET  
458 product for comparison. DF wrote the initial draft and CS revised the manuscript. HB, JdB, RKS, YS, YW, and KL  
459 substantially edited the manuscript.

#### 460 **Financial support**

461 DF was supported by the National Science Foundation Award EAR-2221880. This work was also partially supported and  
462 inspired by the Young Scientists Summer Program (YSSP) of International Institute for Applied Systems Analysis (IIASA).  
463 JL was supported by Google.org's AI Impacts Challenge Grant 1904-57775. CS and KL were supported by Cooperative  
464 Institute for Research to Operations in Hydrology (CIROH), award number A22-0307-S003. Computation was partially  
465 supported by the National Science Foundation Major Research Instrumentation Award PHY-2018280.

#### 466 **Code and Data Availability**

467 The source codes for the differentiable hydrologic models can be accessed at <https://doi.org/10.5281/zenodo.7091334>, and this  
468 study evaluates these models at global scale. The MOD16A2GF ET product can be downloaded at  
469 <https://lpdaac.usgs.gov/products/mod16a2gfv061/>. Meteorological forcing datasets MSWEP and MSWX can be downloaded  
470 at <https://www.gloh2o.org/mswep/> and <https://www.gloh2o.org/mswx/>, respectively. The streamflow observations used in this  
471 study were initially compiled by Beck, Pan, et al., (2020b) and can be accessed from the original data sources including the  
472 United States Geological Survey (USGS) National Water Information System (NWIS; <https://waterdata.usgs.gov/nwis>), the  
473 Global Runoff Data Centre (GRDC; <https://grdc.bafg.de>), the HidroWeb portal of the Brazilian Agência Nacional de Águas  
474 (<https://www.snirh.gov.br/hidroweb>), the European Water Archive (EWA) of EURO-FRIEND-Water  
475 ([https://www.bafg.de/GRDC/EN/04\\_spcldtbss/42\\_EWA/ewa.html](https://www.bafg.de/GRDC/EN/04_spcldtbss/42_EWA/ewa.html)) and the CCM2-JRC CCM River and Catchment Database  
476 (<https://data.jrc.ec.europa.eu/collection/ccm>), Water Survey of Canada (WSC) National Water Data Archive (HYDAT;  
477 <https://wateroffice.ec.gc.ca/>), the Australian Bureau of Meteorology (BoM; <http://www.bom.gov.au/waterdata/>), and the  
478 Chilean Center for Climate and Resilience Research (CR2) website (<https://www.cr2.cl/datos-de-caudales/>).

#### 479 **References**

480 Aboelyzeed, D., Xu, C., Hoffman, F. M., Liu, J., Jones, A. W., Rackauckas, C., Lawson, K., and Shen, C.: A differentiable,  
481 physics-informed ecosystem modeling and learning framework for large-scale inverse problems: demonstration with  
482 photosynthesis simulations, *Biogeosciences*, 20, 2671–2692, <https://doi.org/10.5194/bg-20-2671-2023>, 2023.

483 Alfieri, L., Lorini, V., Hirpa, F. A., Harrigan, S., Zsoter, E., Prudhomme, C., and Salamon, P.: A global streamflow reanalysis  
484 for 1980–2018, *Journal of Hydrology X*, 6, 100049, <https://doi.org/10.1016/j.hydroa.2019.100049>, 2020.

- 485 Beck, H. E., van Dijk, A. I. J. M., de Roo, A., Dutra, E., Fink, G., Orth, R., and Schellekens, J.: Global evaluation of runoff  
486 from 10 state-of-the-art hydrological models, *Hydrology and Earth System Sciences*, 21, 2881–2903,  
487 <https://doi.org/10.5194/hess-21-2881-2017>, 2017a.
- 488 Beck, H. E., Vergopolan, N., Pan, M., Levizzani, V., van Dijk, A. I. J. M., Weedon, G. P., Brocca, L., Pappenberger, F.,  
489 Huffman, G. J., and Wood, E. F.: Global-scale evaluation of 22 precipitation datasets using gauge observations and  
490 hydrological modeling, *Hydrology and Earth System Sciences*, 21, 6201–6217, <https://doi.org/10.5194/hess-21-6201-2017>,  
491 2017b.
- 492 Beck, H. E., van Dijk, A. I. J. M., Levizzani, V., Schellekens, J., Miralles, D. G., Martens, B., and de Roo, A.: MSWEP: 3-  
493 hourly 0.25° global gridded precipitation (1979–2015) by merging gauge, satellite, and reanalysis data, *Hydrology and Earth  
494 System Sciences*, 21, 589–615, <https://doi.org/10.5194/hess-21-589-2017>, 2017c.
- 495 Beck, H. E., Wood, E. F., Pan, M., Fisher, C. K., Miralles, D. G., Dijk, A. I. J. M. van, McVicar, T. R., and Adler, R. F.:  
496 MSWEP V2 Global 3-Hourly 0.1° Precipitation: Methodology and Quantitative Assessment, *Bulletin of the American  
497 Meteorological Society*, 100, 473–500, <https://doi.org/10.1175/BAMS-D-17-0138.1>, 2019.
- 498 Beck, H. E., Wood, E. F., McVicar, T. R., Zambrano-Bigiarini, M., Alvarez-Garretón, C., Baez-Villanueva, O. M., Sheffield,  
499 J., and Karger, D. N.: Bias correction of global high-resolution precipitation climatologies using streamflow observations from  
500 9372 catchments, *Journal of Climate*, 33, 1299–1315, <https://doi.org/10.1175/JCLI-D-19-0332.1>, 2020a.
- 501 Beck, H. E., Pan, M., Lin, P., Seibert, J., Dijk, A. I. J. M. van, and Wood, E. F.: Global fully distributed parameter  
502 regionalization based on observed streamflow from 4,229 headwater catchments, *Journal of Geophysical Research:  
503 Atmospheres*, 125, e2019JD031485, <https://doi.org/10.1029/2019JD031485>, 2020b.
- 504 Beck, H. E., Dijk, A. I. J. M. van, Larraondo, P. R., McVicar, T. R., Pan, M., Dutra, E., and Miralles, D. G.: MSWX: Global  
505 3-hourly 0.1° bias-corrected meteorological data including near real-time updates and forecast ensembles, *Bulletin of the  
506 American Meteorological Society*, 103, E710–E732, <https://doi.org/10.1175/BAMS-D-21-0145.1>, 2022.
- 507 Berghuijs, W. R., Sivapalan, M., Woods, R. A., and Savenije, H. H. G.: Patterns of similarity of seasonal water balances: A  
508 window into streamflow variability over a range of time scales, *Water Resources Research*, 50, 5638–5661,  
509 <https://doi.org/10.1002/2014WR015692>, 2014.
- 510 Bergström, S.: Development and application of a conceptual runoff model for Scandinavian catchments, PhD Thesis, Swedish  
511 Meteorological and Hydrological Institute (SMHI), Norköping, Sweden, 1976.
- 512 Bergström, S.: The HBV model - its structure and applications, Swedish Meteorological and Hydrological Institute (SMHI),  
513 Norrköping, Sweden, 1992.
- 514 Bindas, T., Tsai, W-P., Liu, JT., Rahmani, F., Feng, DP., Bian, YC., Lawson, KE., and Shen, CP Improving large-basin  
515 streamflow simulation using a modular, differentiable, learnable graph model for routing. ESS Open Archive . September 29,  
516 <https://doi.org/10.1002/essoar.10512512.1>  
517
- 518 Burek, P., Satoh, Y., Kahil, T., Tang, T., Greve, P., Smilovic, M., Guillaume, L., Zhao, F., and Wada, Y.: Development of  
519 the Community Water Model (CWatM v1.04) – a high-resolution hydrological model for global and regional assessment of  
520 integrated water resources management, *Geoscientific Model Development*, 13, 3267–3298, <https://doi.org/10.5194/gmd-13-3267-2020>, 2020.
- 522 Chen, B., Krajewski, W. F., Liu, F., Fang, W., and Xu, Z.: Estimating instantaneous peak flow from mean daily flow,  
523 *Hydrology Research*, 48, 1474–1488, <https://doi.org/10.2166/nh.2017.200>, 2017.

- 524 Driscoll, D. G., Carter, J. M., Williamson, J. E., and Putnam, L. D.: Hydrology of the Black Hills Area, South Dakota, 2002.
- 525 Fang, K. and Shen, C.: Near-real-time forecast of satellite-based soil moisture using long short-term memory with an adaptive  
526 data integration kernel, *J. Hydrometeor.*, 21, 399–413, <https://doi.org/10.1175/jhm-d-19-0169.1>, 2020.
- 527 Fang, K., Shen, C., Kifer, D., and Yang, X.: Prolongation of SMAP to spatiotemporally seamless coverage of continental U.S.  
528 using a deep learning neural network, *Geophys. Res. Lett.*, 44, 11,030–11,039, <https://doi.org/10.1002/2017gl075619>, 2017.
- 529 Fang, K., Pan, M., and Shen, C.: The value of SMAP for long-term soil moisture estimation with the help of deep learning,  
530 *IEEE Trans. Geosci. Remote Sensing*, 57, 2221–2233, <https://doi.org/10/gghp3v>, 2019.
- 531 Fang, K., Kifer, D., Lawson, K., Feng, D., and Shen, C.: The data synergy effects of time-series deep learning models in  
532 hydrology, *Water Resources Research*, 58, e2021WR029583, <https://doi.org/10.1029/2021WR029583>, 2022.
- 533 Feng, D., Fang, K., and Shen, C.: Enhancing streamflow forecast and extracting insights using long-short term memory  
534 networks with data integration at continental scales, *Water Resources Research*, 56, e2019WR026793,  
535 <https://doi.org/10.1029/2019WR026793>, 2020.
- 536 Feng, D., Lawson, K., and Shen, C.: Mitigating prediction error of deep learning streamflow models in large data-sparse  
537 regions with ensemble modeling and soft data, *Geophysical Research Letters*, 48, e2021GL092999,  
538 <https://doi.org/10.1029/2021GL092999>, 2021.
- 539 Feng, D., Liu, J., Lawson, K., and Shen, C.: Differentiable, learnable, regionalized process-based models with multiphysical  
540 outputs can approach state-of-the-art hydrologic prediction accuracy, *Water Resources Research*, 58, e2022WR032404,  
541 <https://doi.org/10.1029/2022WR032404>, 2022.
- 542 Feng, D., Beck, H., Lawson, K., and Shen, C.: The suitability of differentiable, physics-informed machine learning hydrologic  
543 models for ungauged regions and climate change impact assessment, *Hydrology and Earth System Sciences*, 27, 2357–2373,  
544 <https://doi.org/10.5194/hess-27-2357-2023>, 2023.
- 545 Gupta, H. V., Kling, H., Yilmaz, K. K., and Martinez, G. F.: Decomposition of the mean squared error and NSE performance  
546 criteria: Implications for improving hydrological modelling, *Journal of Hydrology*, 377, 80–91,  
547 <https://doi.org/10.1016/j.jhydrol.2009.08.003>, 2009.
- 548 Hagemann, S., Chen, C., Clark, D. B., Folwell, S., Gosling, S. N., Haddeland, I., Hanasaki, N., Heinke, J., Ludwig, F., Voss,  
549 F., and Wiltshire, A. J.: Climate change impact on available water resources obtained using multiple global climate and  
550 hydrology models, *Earth System Dynamics*, 4, 129–144, <https://doi.org/10.5194/esd-4-129-2013>, 2013.
- 551 Hansen, L. D., Stokholm-Bjerregaard, M., and Durdevic, P.: Modeling phosphorous dynamics in a wastewater treatment  
552 process using Bayesian optimized LSTM, *Computers & Chemical Engineering*, 160, 107738,  
553 <https://doi.org/10.1016/j.compchemeng.2022.107738>, 2022.
- 554 Hargreaves, G. H.: Defining and using reference evapotranspiration, *Journal of Irrigation and Drainage Engineering*, 120,  
555 1132–1139, [https://doi.org/10.1061/\(ASCE\)0733-9437\(1994\)120:6\(1132\)](https://doi.org/10.1061/(ASCE)0733-9437(1994)120:6(1132)), 1994.
- 556 Hattermann, F. F., Krysanova, V., Gosling, S. N., Dankers, R., Daggupati, P., Donnelly, C., Flörke, M., Huang, S., Motovilov,  
557 Y., Buda, S., Yang, T., Müller, C., Leng, G., Tang, Q., Portmann, F. T., Hagemann, S., Gerten, D., Wada, Y., Masaki, Y.,  
558 Alemayehu, T., Satoh, Y., and Samaniego, L.: Cross-scale intercomparison of climate change impacts simulated by regional  
559 and global hydrological models in eleven large river basins, *Climatic Change*, 141, 561–576, <https://doi.org/10.1007/s10584-016-1829-4>, 2017.

- 561 Hilker, T., Lyapustin, A. I., Hall, F. G., Myneni, R., Knyazikhin, Y., Wang, Y., Tucker, C. J., and Sellers, P. J.: On the  
562 measurability of change in Amazon vegetation from MODIS, *Remote Sensing of Environment*, 166, 233–242,  
563 <https://doi.org/10.1016/j.rse.2015.05.020>, 2015.
- 564 Hochreiter, S. and Schmidhuber, J.: Long Short-Term Memory, *Neural Computation*, 9, 1735–1780,  
565 <https://doi.org/10.1162/neco.1997.9.8.1735>, 1997.
- 566 Höge, M., Scheidegger, A., Baity-Jesi, M., Albert, C., and Fenicia, F.: Improving hydrologic models for predictions and  
567 process understanding using neural ODEs, *Hydrology and Earth System Sciences*, 26, 5085–5102,  
568 <https://doi.org/10.5194/hess-26-5085-2022>, 2022.
- 569 Hou, Y., Guo, H., Yang, Y., and Liu, W.: Global Evaluation of Runoff Simulation From Climate, *Hydrological and Land*  
570 *Surface Models*, *Water Resources Research*, 59, e2021WR031817, <https://doi.org/10.1029/2021WR031817>, 2023.
- 571 Jayakrishnan, R., Srinivasan, R., Santhi, C., and Arnold, J. G.: Advances in the application of the SWAT model for water  
572 resources management, *Hydrological Processes*, 19, 749–762, <https://doi.org/10.1002/hyp.5624>, 2005.
- 573 Jiang, S., Zheng, Y., and Solomatine, D.: Improving AI system awareness of geoscience knowledge: Symbiotic integration of  
574 physical approaches and deep learning, *Geophysical Research Letters*, 47, e2020GL088229,  
575 <https://doi.org/10.1029/2020GL088229>, 2020.
- 576 Kling, H., Fuchs, M., and Paulin, M.: Runoff conditions in the upper Danube basin under an ensemble of climate change  
577 scenarios, *Journal of Hydrology*, 424–425, 264–277, <https://doi.org/10.1016/j.jhydrol.2012.01.011>, 2012.
- 578 Konapala, G., Kao, S.-C., Painter, S. L., and Lu, D.: Machine learning assisted hybrid models can improve streamflow  
579 simulation in diverse catchments across the conterminous US, *Environ. Res. Lett.*, 15, 104022, <https://doi.org/10.1088/1748-9326/aba927>, 2020.
- 581 Kraft, B., Jung, M., Körner, M., Koirala, S., and Reichstein, M.: Towards hybrid modeling of the global hydrological cycle,  
582 *Hydrology and Earth System Sciences*, 26, 1579–1614, <https://doi.org/10.5194/hess-26-1579-2022>, 2022.
- 583 Kratzert, F., Klotz, D., Herrnegger, M., Sampson, A. K., Hochreiter, S., and Nearing, G. S.: Toward improved predictions in  
584 ungauged basins: Exploiting the power of machine learning, *Water Resources Research*, 55, 11344–11354,  
585 <https://doi.org/10/gg4ck8>, 2019a.
- 586 Kratzert, F., Klotz, D., Shalev, G., Klambauer, G., Hochreiter, S., and Nearing, G.: Towards learning universal, regional, and  
587 local hydrological behaviors via machine learning applied to large-sample datasets, *Hydrology and Earth System Sciences*,  
588 23, 5089–5110, <https://doi.org/10.5194/hess-23-5089-2019>, 2019b.
- 589 Lees, T., Buechel, M., Anderson, B., Slater, L., Reece, S., Coxon, G., and Dadson, S. J.: Benchmarking data-driven rainfall–  
590 runoff models in Great Britain: a comparison of long short-term memory (LSTM)-based models with four lumped conceptual  
591 models, *Hydrology and Earth System Sciences*, 25, 5517–5534, <https://doi.org/10.5194/hess-25-5517-2021>, 2021.
- 592 Lees, T., Reece, S., Kratzert, F., Klotz, D., Gauch, M., De Bruijn, J., Kumar Sahu, R., Greve, P., Slater, L., and Dadson, S. J.:  
593 Hydrological concept formation inside long short-term memory (LSTM) networks, *Hydrology and Earth System Sciences*, 26,  
594 3079–3101, <https://doi.org/10.5194/hess-26-3079-2022>, 2022.
- 595 Mai, J., Shen, H., Tolson, B. A., Gaborit, É., Arsenault, R., Craig, J. R., Fortin, V., Fry, L. M., Gauch, M., Klotz, D., Kratzert,  
596 F., O’Brien, N., Princz, D. G., Rasiya Koya, S., Roy, T., Seglenieks, F., Shrestha, N. K., Temgoua, A. G. T., Vionnet, V., and

- 597 Waddell, J. W.: The Great Lakes Runoff Intercomparison Project Phase 4: the Great Lakes (GRIP-GL), Hydrology and Earth  
598 System Sciences, 26, 3537–3572, <https://doi.org/10.5194/hess-26-3537-2022>, 2022.
- 599 Maidment, D. R.: Conceptual Framework for the National Flood Interoperability Experiment, JAWRA Journal of the  
600 American Water Resources Association, 53, 245–257, <https://doi.org/10/f97pz3>, 2017.
- 601 Martinez, G. F. and Gupta, H. V.: Toward improved identification of hydrological models: A diagnostic evaluation of the  
602 “abcd” monthly water balance model for the conterminous United States, Water Resources Research, 46,  
603 <https://doi.org/10.1029/2009WR008294>, 2010.
- 604 Mizukami, N., Clark, M. P., Newman, A. J., Wood, A. W., Gutmann, E. D., Nijssen, B., Rakovec, O., and Samaniego, L.:  
605 Towards seamless large-domain parameter estimation for hydrologic models, Water Resources Research, 53, 8020–8040,  
606 <https://doi.org/10/gcg2dm>, 2017.
- 607 Müller Schmied, H., Eisner, S., Franz, D., Wattenbach, M., Portmann, F. T., Flörke, M., and Döll, P.: Sensitivity of simulated  
608 global-scale freshwater fluxes and storages to input data, hydrological model structure, human water use and calibration,  
609 Hydrology and Earth System Sciences, 18, 3511–3538, <https://doi.org/10.5194/hess-18-3511-2014>, 2014.
- 610 Nash, J. E. and Sutcliffe, J. V.: River flow forecasting through conceptual models part I — A discussion of principles, Journal  
611 of Hydrology, 10, 282–290, <https://doi.org/10/fbg9tm>, 1970.
- 612 Newman, A. J., Mizukami, N., Clark, M. P., Wood, A. W., Nijssen, B., Nearing, G., Newman, A. J., Mizukami, N., Clark, M.  
613 P., Wood, A. W., Nijssen, B., and Nearing, G.: Benchmarking of a Physically Based Hydrologic Model, Journal of  
614 Hydrometeorology, 18, 2215–2225, <https://doi.org/10/gbwr9s>, 2017.
- 615 Niu, J., Shen, C., Chambers, J., Melack, J. M., and Riley, W. J.: Interannual variation in hydrologic budgets in an Amazonian  
616 watershed with a coupled subsurface - land surface process model, Journal of Hydrometeorology, 18, 2597–2617,  
617 <https://doi.org/10.1175/JHM-D-17-0108.1>, 2017.
- 618 Paszke, A., Gross, S., Chintala, S., Chanan, G., Yang, E., DeVito, Z., Lin, Z., Desmaison, A., Antiga, L., and Lerer, A.:  
619 Automatic differentiation in PyTorch, in: 31st Conference on Neural Information Processing Systems (NIPS 2017), Long  
620 Beach, CA, 2017.
- 621 Rahmani, F., Lawson, K., Ouyang, W., Appling, A., Oliver, S., and Shen, C.: Exploring the exceptional performance of a deep  
622 learning stream temperature model and the value of streamflow data, Environ. Res. Lett., 16, 024025,  
623 <https://doi.org/10.1088/1748-9326/abd501>, 2021.
- 624 Running, S., Mu, Q., Zhao, M., and Moreno, A.: MODIS/Terra Net Evapotranspiration Gap-Filled 8-Day L4 Global 500m  
625 SIN Grid V061, <https://doi.org/10.5067/MODIS/MOD16A2GF.061>, 2021.
- 626 Saha, G. K., Rahmani, F., Shen, C., Li, L., and Cibin, R.: A deep learning-based novel approach to generate continuous daily  
627 stream nitrate concentration for nitrate data-sparse watersheds, Science of The Total Environment, 878, 162930,  
628 <https://doi.org/10.1016/j.scitotenv.2023.162930>, 2023.
- 629 Seibert, J. and Vis, M. J. P.: Teaching hydrological modeling with a user-friendly catchment-runoff-model software package,  
630 Hydrology and Earth System Sciences, 16, 3315–3325, <https://doi.org/10/f22r5x>, 2012.
- 631 Shaw, D. A., Pietroniro, A., and Martz, L. w.: Topographic analysis for the prairie pothole region of Western Canada,  
632 Hydrological Processes, 27, 3105–3114, <https://doi.org/10.1002/hyp.9409>, 2013.

- 633 Shen, C.: A transdisciplinary review of deep learning research and its relevance for water resources scientists, *Water Resources*  
634 *Research*, 54, 8558–8593, <https://doi.org/10.1029/2018wr022643>, 2018.
- 635 Shen, C., Appling, A. P., Gentine, P., Bandai, T., Gupta, H., Tartakovsky, A., Baity-Jesi, M., Fenicia, F., Kifer, D., Li, L., Liu,  
636 X., Ren, W., Zheng, Y., Harman, C. J., Clark, M., Farthing, M., Feng, D., Kumar, P., Aboelyazeed, D., Rahmani, F., Song, Y.,  
637 Beck, H. E., Bindas, T., Dwivedi, D., Fang, K., Höge, M., Rackauckas, C., Mohanty, B., Roy, T., Xu, C., and Lawson, K.:  
638 Differentiable modelling to unify machine learning and physical models for geosciences, *Nat Rev Earth Environ*, 4, 552–567,  
639 <https://doi.org/10.1038/s43017-023-00450-9>, 2023.
- 640 Tsai, W.-P., Feng, D., Pan, M., Beck, H., Lawson, K., Yang, Y., Liu, J., and Shen, C.: From calibration to parameter learning:  
641 Harnessing the scaling effects of big data in geoscientific modeling, *Nat Commun*, 12, 5988, [https://doi.org/10.1038/s41467-](https://doi.org/10.1038/s41467-021-26107-z)  
642 [021-26107-z](https://doi.org/10.1038/s41467-021-26107-z), 2021.
- 643 Vanderhoof, M. K., Christensen, J. R., and Alexander, L. C.: Patterns and drivers for wetland connections in the Prairie Pothole  
644 Region, United States, *Wetlands Ecol Manage*, 25, 275–297, <https://doi.org/10.1007/s11273-016-9516-9>, 2017.
- 645 Veldkamp, T. I. E., Zhao, F., Ward, P. J., Moel, H. de, Aerts, J. C. J. H., Schmied, H. M., Portmann, F. T., Masaki, Y., Pokhrel,  
646 Y., Liu, X., Satoh, Y., Gerten, D., Gosling, S. N., Zaherpour, J., and Wada, Y.: Human impact parameterizations in global  
647 hydrological models improve estimates of monthly discharges and hydrological extremes: a multi-model validation study,  
648 *Environ. Res. Lett.*, 13, 055008, <https://doi.org/10.1088/1748-9326/aab96f>, 2018.
- 649 Wunsch, A., Liesch, T., and Broda, S.: Groundwater level forecasting with artificial neural networks: a comparison of long  
650 short-term memory (LSTM), convolutional neural networks (CNNs), and non-linear autoregressive networks with exogenous  
651 input (NARX), *Hydrology and Earth System Sciences*, 25, 1671–1687, <https://doi.org/10.5194/hess-25-1671-2021>, 2021.
- 652 Xu, D., Agee, E., Wang, J., and Ivanov, V. Y.: Estimation of Evapotranspiration of Amazon Rainforest Using the Maximum  
653 Entropy Production Method, *Geophysical Research Letters*, 46, 1402–1412, <https://doi.org/10.1029/2018GL080907>, 2019.
- 654 Yilmaz, K. K., Gupta, H. V., and Wagener, T.: A process-based diagnostic approach to model evaluation: Application to the  
655 NWS distributed hydrologic model, *Water Resources Research*, 44, <https://doi.org/10/fpvsgb>, 2008.
- 656 Zaherpour, J., Gosling, S. N., Mount, N., Schmied, H. M., Veldkamp, T. I. E., Dankers, R., Eisner, S., Gerten, D.,  
657 Gudmundsson, L., Haddeland, I., Hanasaki, N., Kim, H., Leng, G., Liu, J., Masaki, Y., Oki, T., Pokhrel, Y., Satoh, Y., Schewe,  
658 J., and Wada, Y.: Worldwide evaluation of mean and extreme runoff from six global-scale hydrological models that account  
659 for human impacts, *Environ. Res. Lett.*, 13, 065015, <https://doi.org/10.1088/1748-9326/aac547>, 2018.
- 660 Zhi, W., Feng, D., Tsai, W.-P., Sterle, G., Harpold, A., Shen, C., and Li, L.: From hydrometeorology to river water quality:  
661 Can a deep learning model predict dissolved oxygen at the continental scale?, *Environ. Sci. Technol.*, 55, 2357–2368,  
662 <https://doi.org/10.1021/acs.est.0c06783>, 2021.

663